NUMERICAL AND EXPERIMENTAL STUDIES ON AN AERODYNAMIC DISTORTION GRILL

M. Sivapragasam[1], M. D. Deshpande[2], S. N. Sridhara[3] and S. Ramamurthy[4]

Abstract

An aerodynamic distortion grill is employed to create non-uniform flow from arbitrary uniform upstream flow conditions. Such grills find widespread use in aerodynamic testing applications to generate non-uniform flow conditions. In this paper, the numerical results of the distortion created by one such aerodynamic distortion grill are reported. The computational results were validated against the experimentally observed distortion indices. Further, parametric numerical studies were done by varying the inlet turbulence intensity and by scaling up the geometry of the flow system.

Nomenclature

$C_0,...,C_4$ = constants in transducer calibration equation
C_{1e}, C_{2e} = model constants in $k - \varepsilon$ turbulence equations ($C_{1e} = 1.44$, $C_{2e} = 1.92$)
C_μ = constant in turbulence viscosity equation ($C_\mu = 0.09$)
DI = distortion index
I = turbulence intensity
k = turbulence kinetic energy, m^2/s^2
L = length of grill, m ($L = 0.75$m)
M = Mach number
P_s = static pressure, Pa
P_t = total pressure, Pa
W = average velocity, m/s
w' = fluctuating component of velocity, m/s

Greek Symbols

ε = turbulence kinetic energy dissipation rate, m^2/s^3
γ = ratio of specific heats
μ_t = turbulence (eddy) viscosity, kg/m-s
ρ = density, kg/m^3
σ_k, σ_ε = turbulent Prandtl numbers for k and ε, respectively ($\sigma_k = 1.0$, $\sigma_\varepsilon = 1.3$)

Subscripts

avg = average
in = inlet
max = maximum
min = minimum
1L = plane one grill length behind the grill

Introduction

Aerodynamic screens are used in a number of engineering applications, both to remove or create flow non-uniformities. The production of a uniform profile from arbitrary non-uniform upstream conditions is desired for wind-tunnel applications, and the production of a specified non-uniform profile from uniform upstream conditions is required for simulating test conditions. The most common screens used for aerodynamic applications include honeycombs, perforated plates and wire-gauze screens.

The studies on flow through grills can be basically divided into three categories according to Laws and Livesey [1]. The investigations related to the characterisation of the flow properties of the grill fall in the first category. The studies concerning the effect of the grill on time-mean velocity distributions are identified in the second category. The researches pertaining to the turbulence distribution downstream of grill are included in the third category. The aerodynamic grill designed for this study can be listed in the second category, to produce non-uniform flow conditions from uniform upstream conditions.

[1] Research Scholar, Centre for Fluid Flow and Energy Systems Research, Email : msp@msrsas.org [2] Head, Research
[3] Head, Department of Mechanical and Automotive Engineering, MS Ramaiah School of Advanced Studies, Bangalore-560 054, India
[4] Scientist, Propulsion Division, National Aerospace Laboratories, Post Box No. 1779, Bangalore-560 017, India
Manuscript received on 30 Oct 2007; Paper reviewed, revised and accepted on 22 Apr 2008

An aerodynamic grill, which is basically a perforated plate, consists of a regular arrangement of narrow passages through which the fluid passes and meets a sudden enlargement on the downstream face. This grill is placed at right angles to a steady stream and fluid discharges from the rear of the grill as a number of jets, which ultimately mix with the surrounding fluid and form a uniform stream again, as described by Batchelor [2]. The studies reported in the present paper were aimed at investigating this fluid mixing and the associated total pressure loss, which corresponds to a distortion pattern.

The primary objectives of this study were to understand the mechanism of loss in total pressure due to mixing and its effect on the distortion index. It was desired to evaluate a non-dimensional loss coefficient associated with the mixing loss. In effect to achieving these objectives, studies were conducted on an aerodynamic distortion grill at different inlet Mach numbers and different inlet turbulence intensities. The effect of scaling on the distortion index was also evaluated. Such a study on a rather simple geometry aerodynamic grill would throw light on the fluid dynamic phenomena associated with fluid mixing influencing the total pressure loss. The results would considerably aid in the design of screens to produce prescribed distortion patterns for simulating test conditions.

The flowfield behind the aerodynamic distortion grill was numerically analysed using the Navier-Stokes code, FLUENT, Version 6.1.26. The results were compared with the experiments conducted at the Closed Circuit Centrifugal Test Rig (CLOCTER) Facility at the Propulsion Division of National Aerospace Laboratories. Further, parametric studies were conducted numerically by varying the inlet turbulence intensity and by appropriately scaling the geometry of the flow system.

Numerical Studies

Grill Geometry

The aerodynamic grill designed for the investigation is shown in Fig. 1. The square grill of side 75 mm had nine equi-spaced square holes of size 20 mm x 20 mm. The web width was 5 mm and the thickness of the grill was 5 mm.

The Computational Fluid Dynamics solver FLUENT, is a finite-volume based code for fluid flow simulations [3]. The fundamental idea is to discretise the governing equations of fluid dynamics namely the mass, momentum and energy conservation equations, which are listed below:

$$\frac{\partial \rho}{\partial t} + \frac{\partial}{\partial x_i}(\rho v_i) = 0 \quad (1)$$

$$\frac{\partial \rho}{\partial t}(\rho v_i) + \frac{\partial}{\partial x_i}(\rho v_j v_i) = \rho F_i - \frac{\partial p}{\partial x_i} + \frac{\partial}{\partial x_i}\tau_{ij} \quad (2)$$

$$\frac{\partial}{\partial t}\left[\rho\left(e+\frac{1}{2}v^2\right)\right] + \frac{\partial}{\partial x_i}\left[\rho v_i\left(e+\frac{1}{2}v^2\right)\right]$$

$$= -\frac{\partial}{\partial x_i} q_i + \frac{\partial}{\partial x_i}(\tau_{ij} v_j) + \rho v_i F_i \quad (3)$$

The conservation equations are discretised to algebraic equations that can be solved numerically for fluid component velocities, density, pressure, and temperature parameters. The linearised algebraic equations are solved iteratively until a converged solution is achieved.

Computational Domain

The first step towards obtaining a numerical solution for the governing equations is the spatial discretisation of the fluid domain. The fluid domain is divided into a number of small contiguous computational cells or control volumes. The grill geometry was created in the pre-processing software GAMBIT. The upstream domain was at 75 mm from the inlet of the grill and the downstream domain extended up to 225 mm from the exit of the grill. The entire fluid domain was meshed with hexahedral cells.

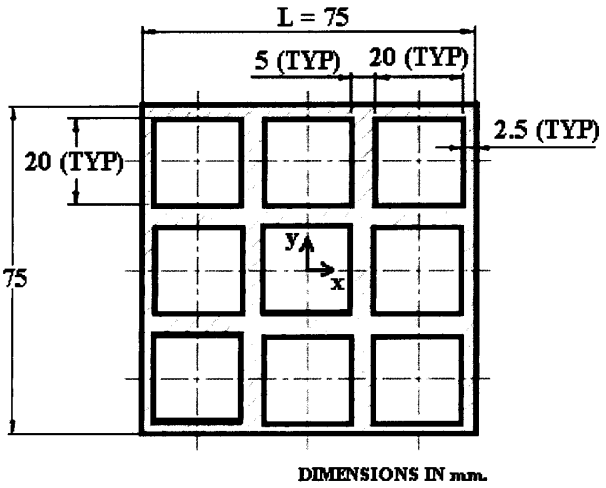

Fig.1 Grill geometry

Boundary Conditions

The boundary zones specified for the discretised model were specified as illustrated in Fig. 2.

The pressure inlet boundary condition was imposed at the inlet of the domain. The inlet total pressure and all the other scalar properties of the flow were specified at the inlet. The outlet static pressure was specified at the outlet boundary. The inlet total pressure and the outlet static pressure boundary conditions were used in conjunction to vary the inlet Mach number. On the external walls bounding the flow domain the 'no-slip', 'no-penetration' conditions on the fluid were specified.

Solver Settings

The segregated-implicit solver setting in FLUENT was activated to obtain the converged solutions. The segregated solver solves the mass, momentum and energy conservation equations sequentially. The first-order upwind scheme was employed to discretise the governing equations. This scheme was considered suitable and sufficient as the flow was aligned with the computational grid. All calculations were carried out in double-precision arithmetic. The imbalance of mass between the inlet and outlet were monitored closely and the convergence criterion on the continuity equation was set to 10^{-7}.

Turbulence Model

The turbulence model approach is a very practical way of treating turbulent flows. A hierarchy of turbulence models are made available in FLUENT. The standard *k*-ε model was chosen for the solution of the problem since it is generally believed to be satisfactory for a wide class of problems and is widely validated.

The turbulence (or eddy) viscosity, μ_t is calculated as,

$$\mu_t = \rho C_\mu \frac{k^2}{\varepsilon} \tag{4}$$

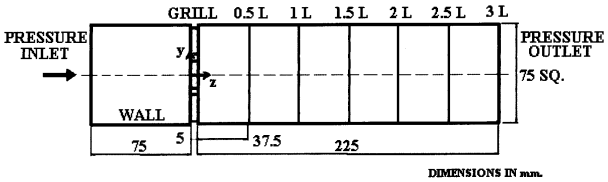

Fig.2 Computational domain and measurement planes

where C_μ is a constant. The model constants are assigned the following values:

$$C_{1e} = 1.44,\ C_{2e} = 1.92,\ C_\mu = 0.09,\ \sigma_k = 1.0,\ \sigma_\varepsilon = 1.3$$

Distortion Index

The principal parameter of interest in these studies is the Distortion Index, which is defined for a plane as,

$$\text{Distortion Index} = \frac{P_{t,\max} - P_{t,\min}}{P_{t,\text{avg}}} . \tag{5}$$

This non-dimensional parameter quantifies the non-uniformity of flow in the duct. This description of distortion is very useful for comparative purposes as indicated by Seddon and Goldsmith [4]. The distortion index was evaluated at various planes downstream of the grill identified in Fig. 2.

Loss Coefficient

The total pressure loss due to the grill and consequent mixing was quantified by a global non-dimensional parameter called the Loss Coefficient, which is defined as,

$$\text{Loss Coefficient} = \frac{P_{t,\text{in}} - P_{t,1L}}{\tfrac{1}{2}\rho_{\text{in}} V_{\text{in}}^2} \tag{6}$$

where $P_{t,1L}$ is the average total pressure at a plane one grill length behind the aerodynamic grill as shown in Fig. 2.

Averaging non-uniform flows is important for the analysis of measurements in internal flow applications. Data averaging can be carried out by various methods, the area-weighted, mass-weighted and momentum-weighted averaging techniques being commonly used. Recently, Cumpsty and Horlock [5] revisited this fundamentally important problem and have shown that the numerical differences for different types of averaging are small for many cases. The mass-weighted averaging was used in the present study as is generally practised.

Grid Sensitivity Analysis

The number of computational cells used in the CFD analysis determines the accuracy of the solution. The use

of fine mesh improves the accuracy of the simulation but at the expense of higher computational effort. Hence, grid sensitivity analysis is performed to obtain an optimum number of computational cells. The flow domain was initially meshed with 38510 cells to simulate the flowfield and assess the solver settings. The number of cells was subsequently increased to 188500, 358000, 602640 and finally to 913280. The results are shown in Fig. 3 where the distortion indices at various planes downstream of the grill are plotted for different mesh sizes. It was observed that the distortion indices evaluated at all the planes were insensitive to the number of cells in the computational domain. It was decided to conduct all further CFD analysis with 358000 number of computational cells.

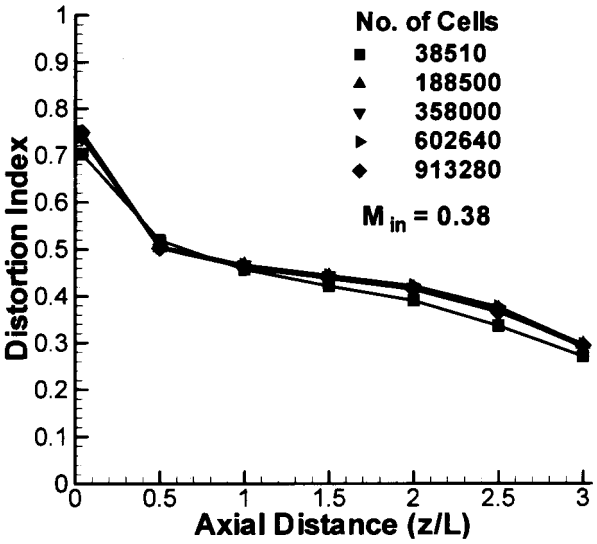

Fig.3 Grid sensitivity analysis

Variation of Distortion Index with Inlet Mach Number

The distortion index was evaluated at various planes for different inlet Mach numbers. The static pressure at the outlet was varied to alter the inlet Mach number. The inlet Mach number was varied from 0.09 to 0.39. The variation of distortion index for different inlet Mach numbers is shown in Fig. 4a.

It was observed that the distortion index increased with an increase in inlet Mach number. The maximum distortion index occurred at the plane just downstream of the grill. Inlet Mach number was found to be 0.38 when the flow reached the local sonic condition in the holes. A further decrease in the outlet static pressure is required for the holes to choke completely. At choked condition, the distortion index at the other planes reached their peak values too. The variation of distortion index downstream of the grill for different inlet Mach numbers is plotted in Fig. 4b. It was noted that the peak distortion index occurred in the plane just downstream of the grill at the choked condition. At planes far downstream of the grill a substantial decrease in the distortion index was observed as the flow had mixed with a tendency to become uniform again.

The total pressure distortion decay pattern obtained due to the aerodynamic grill is shown in Fig. 5. The total pressure was normalised by the inlet total pressure. The

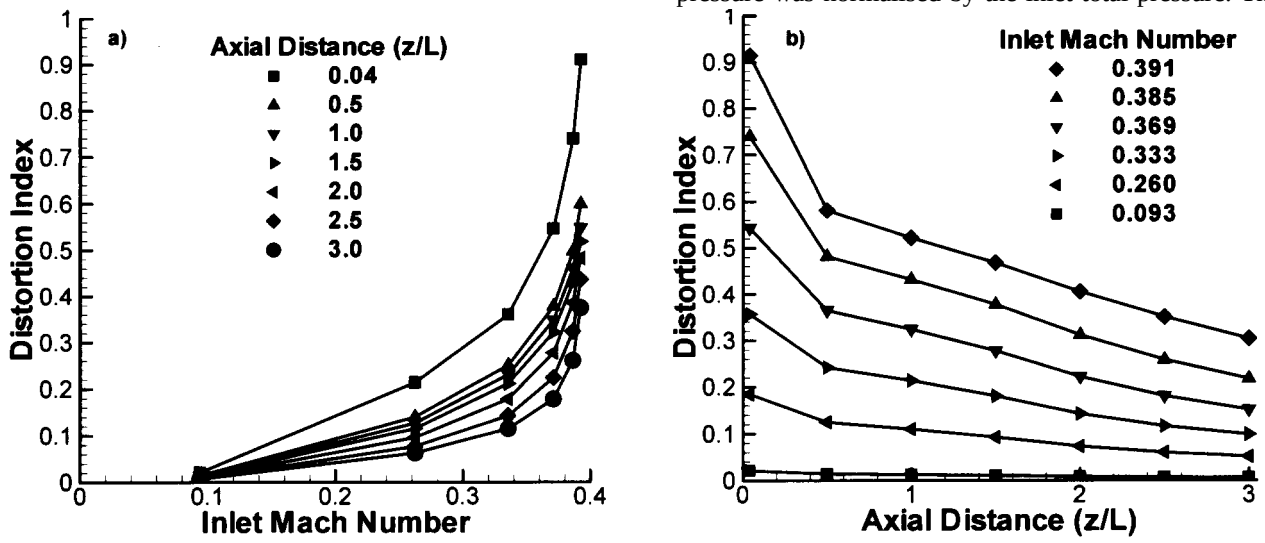

Fig.4 Variation of distortion index with inlet Mach number

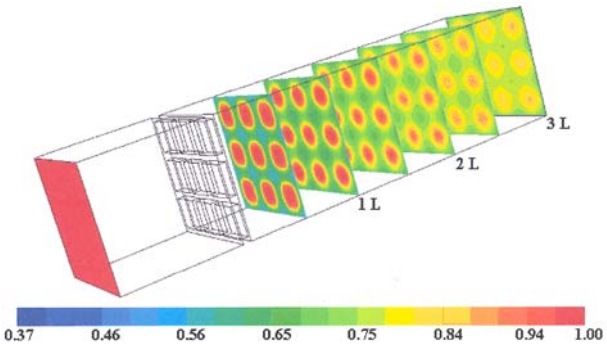

Fig.5 Contours of normalised total pressure ($P_t/P_{t,in}$) behind distortion grill

inlet Mach number was 0.38. It can be seen that the nine axial jets issuing out of the holes in the grill start mixing. On the plane just downstream of the grill, the contour plot clearly indicates that the distortion is quite high. At the outlet of the domain, the jets have mixed out and the flow has become more uniform.

Variation of Loss Coefficient with Inlet Mach Number

The loss coefficient was a means of evaluating the total pressure loss due to fluid mixing. The loss coefficient was calculated for varying inlet Mach numbers and the resulting plot is shown in Fig.6. As was expected, the loss coefficient was low for low inlet Mach numbers. The highest loss coefficient was calculated at an inlet Mach number corresponding to choking of the holes in the grill.

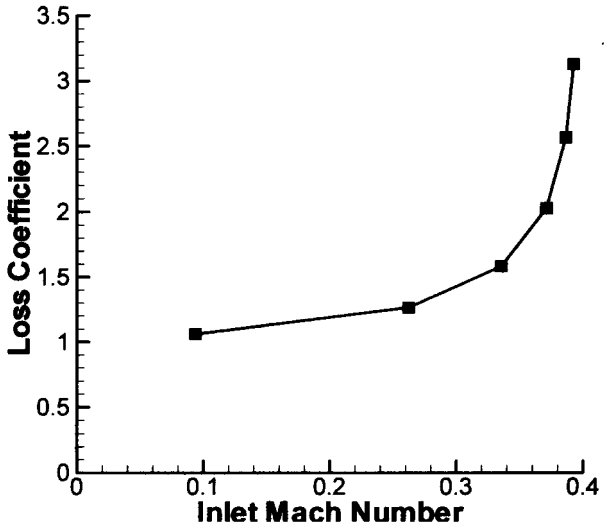

Fig.6 Variation of loss coefficient with inlet Mach number

Experimental Studies

The experimental facility was set up at the Closed Circuit Centrifugal Compressor Test Rig (CLOCTER) Facility at the Propulsion Division of National Aerospace Laboratories.

Experimental Facility

The schematic of the experimental set up is shown in Fig. 7. High-pressure compressed air was sourced from the central Compressed Air Facility. A 50.8 mm (2") ball valve was installed in the line to control the mass flow into the system. A 3.5 m long 50.8 mm diameter pipe was

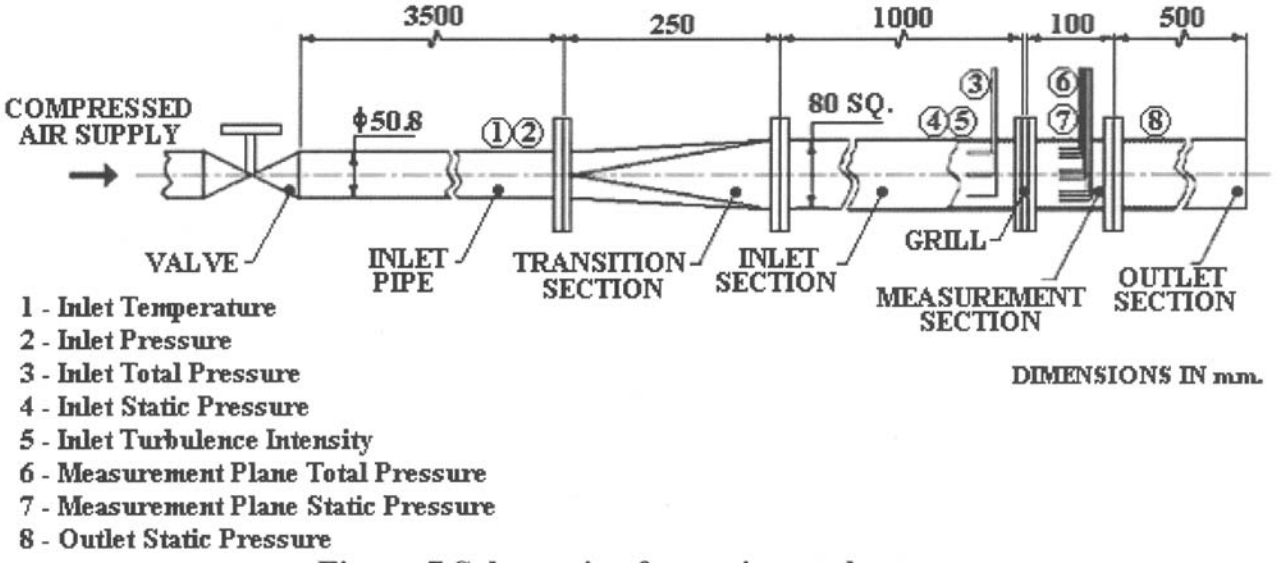

Fig.7 Schematic of experimental set up

installed to attain fully developed flow. The inlet pressure to the system was monitored on a Heise pressure gauge. A Chromel-Alumel thermocouple was installed in this pipe to observe the inlet total temperature. A transition section with minimal divergence angle (approximately 3.5°) was employed to transition the flow from 50.8 mm diameter pipe to 80 mm square section. The flow became fully developed after the transition section in the inlet section. The inlet section was 1 m long and the inlet instrumentation was mounted on this square duct. The inlet total pressure was surveyed by nine equi-spaced probes on three rakes. The rakes (indicated by number 3 in Fig.7) were fixed 37.5 mm ahead of the aerodynamic grill. Exactly on the same plane, four static pressure taps were drilled on the four walls. A hot-wire anemometer was used to measure the inlet turbulence intensity. The hot-wire anemometer was positioned at the same upstream distance, but between two rakes.

The aerodynamic grill was installed between the inlet section and the measurement section. The pressure distortion caused by the grill was measured by 27 total pressure probes on three rakes. The rakes were designed in such a manner that the pressure distribution could be measured by three probes for each jet issuing from the holes in the grill. These rakes were installed 37.5 mm downstream of the grill. The static pressure taps were drilled on the same plane on the four walls. The outlet section was 500 mm long and served to exit the air to the atmosphere. The outlet static pressure was measured by four taps drilled on the walls in a plane 100 mm from its flange. All the ducts (circular and square) were fabricated out of commercial grade mild steel material. With this set up, the distortion can be measured at 0.5 grill length (37.5 mm) behind the grill. The distortion at planes further downstream was measured by inserting extension sections in between the grill and the measurement plane. The extension sections were made in lengths of 37.5 mm, 75 mm and 112.5 mm. When installed in appropriate combination, distortion at all planes of interest can be measured.

Pressure Measurement

An ESP 32-HD miniature pressure scanner was used for the measurement of pressures. It consists of an array of 32 silicon piezo-resistive pressure sensors embedded in the system. The analog outputs are multiplexed and amplified within the scanner. The amplification is done via an internal instrumentation amplifier to provide a nominal full-scale output of ±4 V DC. The pressure sensors were calibrated as per the instructions given in ESP Miniature Pressure Scanner-User's Manual [6]. The calibration of the sensors was done by pneumatically switching the scanner calibration manifold into the calibrate position by applying a pressure of 100 psig (700 kPa). The zero offset of the transducers was obtained by exposing the transducers to atmospheric pressure through a common port. The calibration pressures were applied from a Druck Pressure Calibrator from 5 psi (35 kPa) to 25 psi (172 kPa), in steps of 5 psi (35 kPa). The corresponding output from the transducers in millivolts was noted. A fourth-order polynomial resulting from a five-point calibration was used to calculate the pressure during data acquisition. The polynomial is of the form,

$$P_x = C_0 + C_1 (V_x) + C_2 (V_x)^2 + C_3 (V_x)^3 + C_4 (V_x)^4 \quad . (7)$$

A program was written in TransEra HTBasic to carry out the curve fitting and to obtain the five constants in this equation. Two pressure scanners were used and a total of 64 pressure sensors were individually calibrated.

Data Acquisition and Processing

An Agilent 34970A Data Acquisition/Switch Unit [7] was employed to acquire the data from the pressure transducers. A PC-based Data Acquisition and Reduction Program was interfaced to the Data Acquisition/Switching Unit through a general-purpose interface bus (GPIB). A program was written in TransEra HTBasic to reduce and post-process the data. The program acquires the calibration coefficients from the saved data file. The voltages are acquired from both the transducers and are converted to pressures using the calibration coefficients. The inlet total pressure is the average from the total pressures of the nine probes; the inlet static pressure is the average of the four wall static pressures. The inlet Mach number is calculated from the static and total pressures measured at the inlet plane using the isentropic relation,

$$M_{in} = \left\{ \frac{2}{\gamma - 1} \left[\left(\frac{P_{t,in}}{P_{s,in}} \right)^{\gamma - 1/\gamma} - 1 \right] \right\}^{0.5} \quad . \qquad (8)$$

The minimum, maximum and the average pressures in the distortion plane are evaluated and the distortion index is calculated as defined earlier. The pressures, inlet temperature, inlet Mach number and the distortion index are displayed on the computer monitor and are written to a file for documentation.

Results

The flow uniformity in the experimental set up was checked before the actual measurements were taken by surveying the pressure field without the aerodynamic grill. This was done by taking measurements in the inlet and the distortion measurement plane ($z = 1L$) for different inlet Mach numbers ranging from 0.25 to 0.38. The maximum distortion index values were found to be less than 0.01 in the inlet plane and less than 0.02 in the distortion measurement plane. These results show satisfactory flow uniformity levels in the duct.

The experimentally measured distortion index was checked for repeatability. This was done to verify if the same distortion indices were obtained for the same inlet Mach number for experiments conducted at different times. The results from this exercise showed that the test data had a high degree of repeatability.

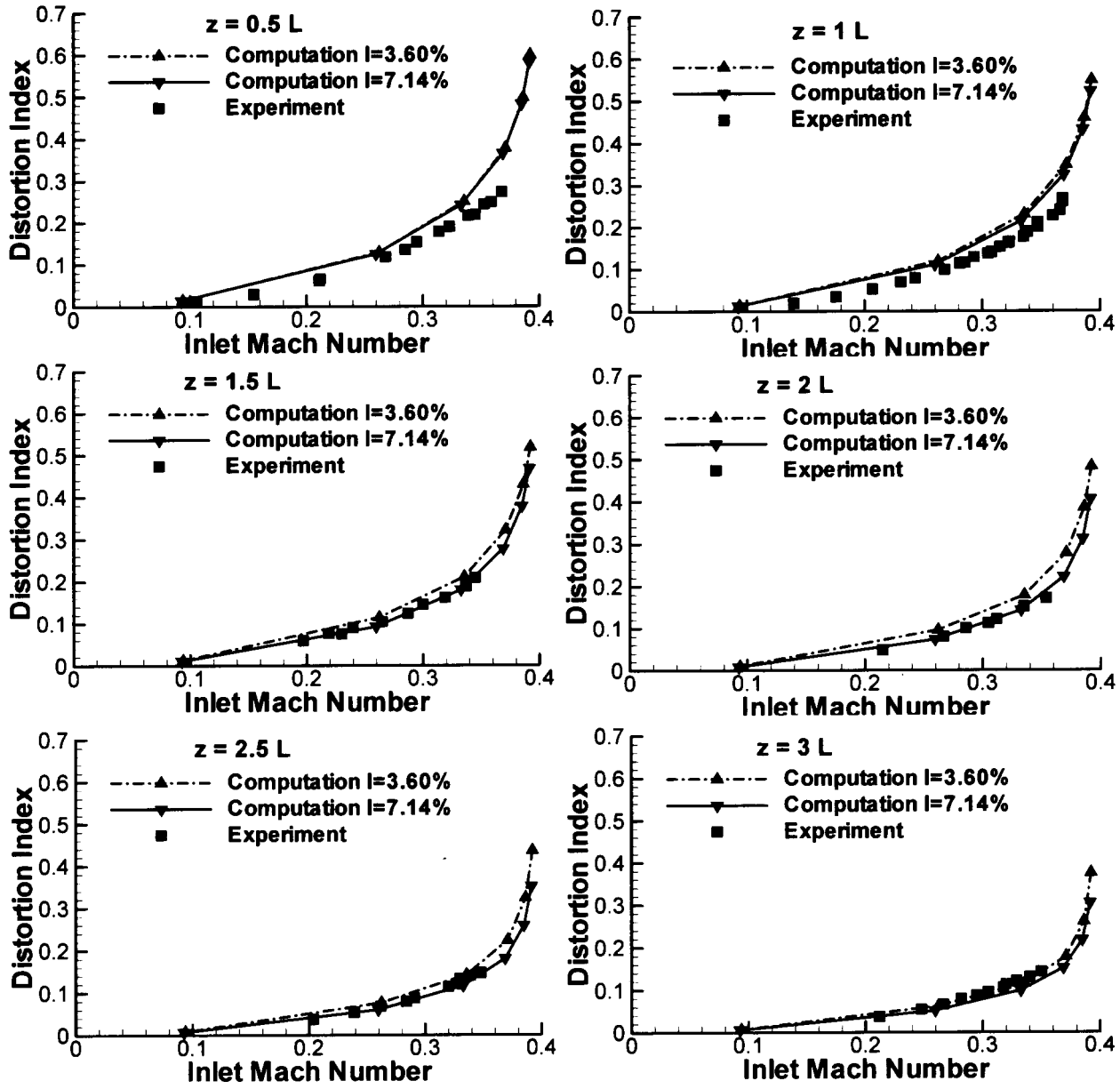

Fig.8 Comparison of computational and experimental results

The distortion immediately downstream of the grill was not measured, as this was found not feasible. The experimentally observed distortion index at various other planes behind the grill is shown in Fig. 8. Initially, computational studies were done for an inlet turbulence intensity of 3.6%, which was calculated based on an empirical relation for fully developed pipe flows. But the inlet turbulence intensity that was measured in the experimental set up was 7.14%. Later, this inlet turbulence intensity was input for the computation and results were obtained. The computational results for 3.6% inlet turbulence intensity are also plotted in Fig. 8 for comparison. The distortion index evaluated computationally and that measured experimentally agree well except just behind the grill at a Mach number close to choking of the holes. The difference between the computational and experimental results may be due to the slight inlet flow non-uniformity and unsteadiness in the experimental set-up. It may be noted that agreement between computational and experimental results improves at planes further downstream of the grill.

While conducting the experiments, it was observed that the holes in the aerodynamic grill choked at an inlet Mach number of 0.36, while the inlet Mach number corresponding to choking of the holes in the computation was 0.38. Thus, it was not possible to experimentally verify the peak distortion index evaluated from numerical simulations.

An analysis of the measurement uncertainty for the calculated inlet Mach number and distortion index is presented in Appendix A.

Parametric Numerical Studies

With the experience and confidence gained from the computational and experimental analysis of the distorted flowfield generated by the aerodynamic distortion grill, a set of parametric numerical analysis was embarked upon to study the flowfield behind the grill. The parametric studies included the variation of inlet turbulence intensity and effect of geometric scaling of the grill.

Variation of Distortion Index with Inlet Turbulence Intensity

The turbulence intensity is defined as ratio of the root-mean-square of the velocity fluctuations to the average flow velocity; see Hinze [8].

$$I = \frac{w'}{W} \quad . \tag{9}$$

The relationship between the turbulence kinetic energy, k, and turbulence intensity, I, assuming turbulence to be isotropic, is,

$$k = \frac{3}{2}(WI)^2 \quad . \tag{10}$$

Turbulence intensity of 1% or less is generally considered low, and turbulence intensities greater than 10% are high. The distortion index was obtained at various planes for different inlet turbulence intensities at an inlet Mach number of 0.33. The inlet turbulence intensity was varied from 1% to 10%. Results are plotted for select values of inlet turbulence intensity in Fig. 9.

It may be seen that the distortion index did not vary much up to one grill length behind the grill with varying inlet turbulence intensity. This region was dominated by fluid mixing. Further downstream, the distortion index took low values for higher turbulence intensities. As may be expected, the high turbulence level resulted in better momentum transport in the transverse direction resulting in more uniform flow and low distortion levels. This fact can be readily ascertained by studying the variation of loss coefficient with inlet turbulence intensity. This is plotted in Fig. 10. As expected, it was found that the loss coefficient increased with increasing turbulence intensity. The momentum transport had made the flow more uniform and had resulted in a lower mass-weighted average total pressure at Plane 1L at high turbulence intensity.

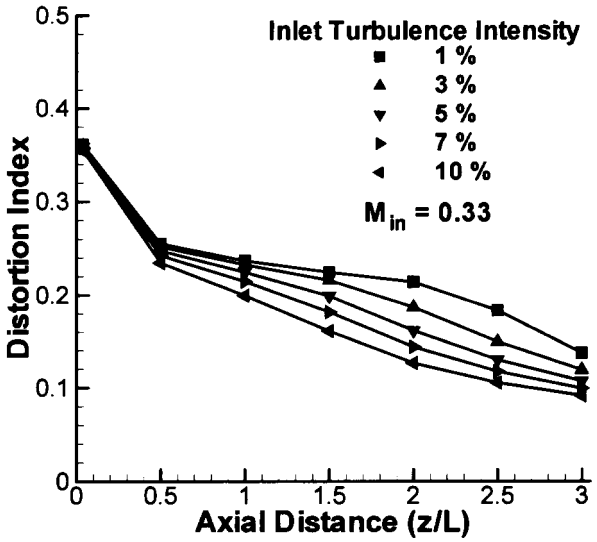

Fig.9 Variation of distortion index with inlet turbulence intensity

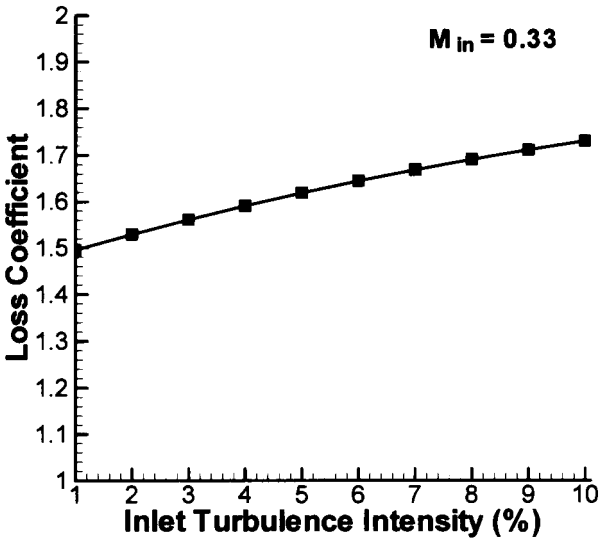

Fig.10 Variation of loss coefficient with inlet turbulence intensity

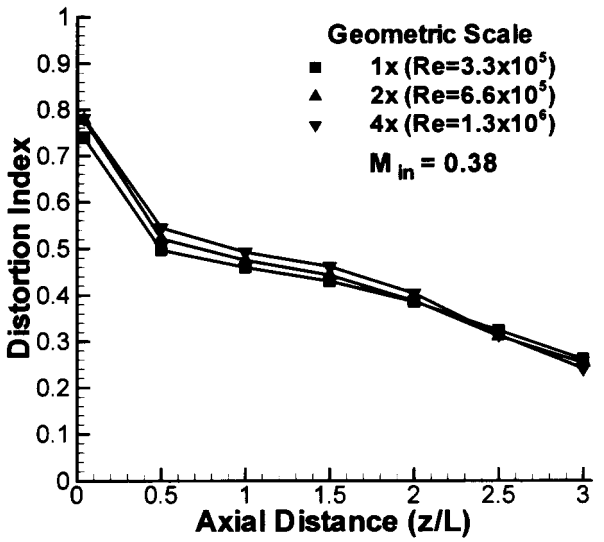

Fig.11 Variation of distortion index with geometric scale

Effect of Scaling on Distortion Index

The effect of scaling on the distortion index was also one of the objectives of this research. This study seemed essential because experiments are usually conducted on small-scale models. It was desired to examine if scaling up the grill geometry had any effect on the distortion index behind the aerodynamic grill. Computations were done on two scaled up models (2x and 4x). This was equivalent to increasing the Reynolds number twice and four times respectively. The Reynolds numbers were calculated based on the hydraulic diameter of the square duct and the mean inlet velocity. The number of cells used for the computation of 1x, 2x and 4x geometries are 358000, 729120 and 1342720 respectively.

The results obtained are plotted in Fig. 11. The analysis was done for the same inlet Mach number for all the three cases. The distortion indices are plotted for the original geometry and the scaled up geometries. As the geometry was scaled up, it was observed that the distortion index increased only slightly.

Conclusions

The distortion pattern behind the aerodynamic grill was evaluated both computationally and experimentally. The results obtained were in good agreement. It was observed that even a simple grill, as the one considered here could produce considerable distortion in the total pressure.

The distortion index and loss coefficient were evaluated for different inlet Mach numbers. It was found that both these parameters were highly dependent on the inlet Mach number and had reached their peak values at an inlet Mach number corresponding to choking of holes in the grill. This result was verified both computationally and experimentally. The power of CFD was exploited further in the form of parametric studies by extending the calculations to different values of turbulence intensity and to geometric scaling. It was seen that at high turbulence intensity the distortion index at all planes was low. The effect of geometric scaling or Reynolds number on the distortion index was evaluated and was found to be small.

A methodology was devised and thoroughly validated to numerically simulate the flowfield behind aerodynamic distortion screens. This methodology can be employed to analyse the flowfield behind complex distortion screens designed to produce prescribed distortion patterns.

Acknowledgements

The authors thank the scientists and staff at the Closed Circuit Centrifugal Compressor Test Rig (CLOCTER) Facility and the Special Purpose Workshop, Propulsion Division, National Aerospace Laboratories for their tremendous support during the experimental work.

References

1. Laws, E. M. and Livesey, J. L., "Flow Through Screens", Annu. Rev. Fluid Mech., Vol. 10, 1978, pp. 247-266.

2. Batchelor, G. K., An Introduction to Fluid Dynamics, Cambridge University Press, Cambridge, 1967.

3. Fluent Users Guide, Version 6.2, Fluent Inc., Lebanon, NH, 2005.

4. Seddon, J. and Goldsmith, E. L., "Intake Aerodynamics", Collins, London, 1985.

5. Cumpsty, N. A. and Horlock, J. H., "Averaging Nonuniform Flow for a Purpose", ASME J. Turbomach., Vol. 128, No. 1, 2006, pp. 120-129.

6. "ESP-Miniature Pressure Scanners", User's Manual, Pressure Systems Inc., Virginia, 1999.

7. Agilent 34970A Data Acquisition/Switch Unit-User Guide, Edition 3, Agilent Technologies, 1999.

8. Hinze, J. O., Turbulence, Second Edition, Mc-Graw Hill, New York, 1975.

9. Kline, S. J. and McClintock, F. A., "Describing Uncertainties in Single-Sample Experiments", Mech. Engg., Vol. 75, No. 1, 1953, pp. 3-8.

Appendix A

Analysis of Measurement Uncertainty

An analysis of the measurement uncertainty for the calculated inlet Mach number and distortion index was done following the method of Kline and McClintock [9]. In the experiments conducted, the inlet Mach number and distortion index were calculated from the pressure measurements. The accuracy of the pressure sensors specified by the manufacturer was ±0.05% full scale. This was taken as the uncertainty in the individual pressure measurements. Substituting appropriate values from the experimental data corresponding to typical inlet Mach numbers and distortion index, the calculated uncertainty is presented in Table- 1.

Table-1 : Uncertainty in the calculated parameters

Inlet. Mach. Number, M_{in}	Uncertainty in Inlet Mach Number, $U(M)_{in}$ (%)	Distortion Index, *DI*	Uncertainty in Distortion Index, $U(DI)$ (%)
0.240	0.202	0.089	6.897
0.299	0.150	0.145	6.792
0.345	0.118	0.209	6.682